



# A self-elastic chitosan sponge integrating active and passive hemostatic mechanisms for effectively managing uncontrolled coagulopathic hemorrhage

Xinchen Du<sup>a,b,1</sup>, Tongxing Zhang<sup>c,1</sup>, Yadong Liu<sup>a</sup>, Tong Li<sup>c</sup>, Jiuxia Yang<sup>d</sup>, Xuelei Li<sup>a,\*</sup>, Lianyong Wang<sup>b,\*\*</sup>

<sup>a</sup> Department of Chemical and Environmental Engineering, Hetao College, Bayannaer, Inner Mongoli, 015000, China

<sup>b</sup> Key Laboratory of Bioactive Materials, Ministry of Education, College of Life Sciences, Nankai University, Tianjin, 300071, China

<sup>c</sup> Department of Minimally Invasive Spine Surgery, Tianjin Hospital, Tianjin University, No. 406, Jiefangnan Road, Hexi District, Tianjin, 300211, China

<sup>d</sup> Key Laboratory of Critical Care Medicine, Tianjin First Central Hospital, Tianjin, 300071, China

## ARTICLE INFO

### Keywords:

Thrombin  
Self-elastic chitosan sponge  
Rapid shape recovery  
Uncontrolled coagulopathic hemorrhage  
Hemostasis

## ABSTRACT

Developing a self-elastic sponge integrating active and passive hemostatic mechanisms for the effective management of uncontrolled coagulopathic hemorrhage remains a challenge. We here developed a chitosan-based sponge by integrating freeze-drying, chemical decoration of alkyl chains and phosphate groups, and physical loading of thrombin. The sponge exhibited high mechanical strength, self-elasticity, and rapid shape recovery. The sponge facilitated blood cell adhesion, aggregation, and activation through hydrophobic and electrostatic interactions, as well as accelerated blood clotting. The sponge exhibited higher efficacy than commercial gauze and gelatin sponge in managing uncontrolled hemorrhage from heparinized rat tail amputation, liver superficial injury, and liver perforating wound models. In addition, the sponge exhibited favorable biodegradability and biocompatibility. These findings revealed that the developed sponge holds great potential as a novel hemostat for effectively managing uncontrolled coagulopathic hemorrhage from superficial and perforating wounds.

## 1. Introduction

Massive hemorrhage is the primary cause of trauma-related morbidity and mortality [1–3]. Although various hemostatic agents (e. g., QuikClot, HemCom bandage, and Celox powder) have demonstrated high efficacy in managing minor hemostasis [4,5], managing uncontrolled (massive) hemorrhage from superficial and perforating wounds, especially in patients with coagulopathy (coagulopathy is a condition in which the blood's ability to form clots is impaired due to genetic disorder, chronic disease, or medications), remains a challenge [2,4]. Therefore, a hemostatic agent suitable for those wounds must be developed. An ideal hemostatic agent should integrate active and passive hemostatic mechanisms [6,7]. The active mechanism is the ability of the agent to promote blood cell adhesion, aggregation, and activation, as well as initiate the body's intrinsic coagulation cascade process [8,9], while the passive mechanism refers to its physical concentration effect

on blood components and its mechanical compression effect on the bleeding site [10–13].

The shape-memory sponges have been proven to be highly efficient in managing uncontrolled hemorrhage, especially for perforating wounds [14–16]. XStat™, as a commercial hemostat containing compressed cellulose sponges, can rapidly expand following water absorption and apply mechanical pressure on the wound to control hemorrhage [17]. However, it cannot strongly interact with blood cells or activate the body's intrinsic coagulation cascade process, leading to the occurrence of challenging -to-control severe hemorrhage. Moreover, Guo and others have developed a series of shape-memory cryogels or sponges [18–21]. Although they can facilitate blood cells adhesion, aggregation, and activation or activate the body's intrinsic coagulation cascade process, their shape recovery property needs to be further improved to achieve more efficient hemostasis. For example, they require a long time to recover the original shapes, and their shape recovery time is

\* Corresponding author.

\*\* Corresponding author.

E-mail addresses: [1094994696@qq.com](mailto:1094994696@qq.com) (X. Li), [wly@nankai.edu.cn](mailto:wly@nankai.edu.cn) (L. Wang).

<sup>1</sup> These authors contributed equally.

significantly prolonged after coming in contact with high-viscosity blood, causing untimely wound compression and massive blood loss. A novel hemostatic sponge integrating active and passive (rapid shape recovery, even when comes in contact with high-viscosity blood) hemostatic mechanisms is therefore highly desired.

Chitosan (CS) is a cationic polysaccharide produced through chitin deacetylation [20,22]. CS can promote blood cells adhesion, aggregation, and activation by intensive electrostatic interactions [23]. CS contains abundant amino groups, facilitating subsequent modifications with functional groups to increase its hemostatic capacity [24]. Moreover, CS can be prepared in a sponge form to absorb water within the blood, concentrate blood components, and load coagulation factors [25]. Additionally, CS can be degraded by lysozyme in the body, and the degradation products are non-toxic and have no side effects [5,10]. These properties render CS an excellent matrix material for the preparation of hemostatic agent.

Red blood cell (RBC) and platelet are vital for physiological hemostasis, as they regulate blood flow, form barriers, facilitate platelet adhesion/aggregation in the fibrin network, form a platelet embolus, and release coagulation factors to accelerate clotting [3,24]. The cell membranes of RBC and platelet contain abundant positive charge groups (e.g., quaternary ammonium groups of phosphatidylcholine) and hydrophobic regions composed of alkyl chains [26]. Therefore, it is reasonable to assume that a hemostatic sponge that can interact electrostatically and hydrophobically with RBC and platelet would be highly

effective in managing uncontrolled coagulopathic hemorrhage.

This study aimed to develop a novel hemostatic sponge integrating active and passive hemostatic mechanisms to effectively manage uncontrolled coagulopathic hemorrhage. The self-elastic CS sponge was first prepared using the freeze-drying method (Fig. 1A). The alkyl chains and phosphate groups were then covalently decorated onto the surface of the CS sponge through an amidation reaction between the amino groups of CS and NHS groups of DSPE-PEG-NHS (Fig. 1A–C). We hypothesized that these decorated groups can engage in hydrophobic and electrostatic interactions with blood cells (Fig. 1B), thereby promoting their adhesion, aggregation, and activation, and accelerating coagulation. Thereafter, thrombin was loaded into the chemically decorated CS (DSPE-CS) sponge through physical absorption for conferring it with the ability to activate the body's intrinsic coagulation cascade process. Various physical properties (e.g., microstructure, porosity, liquid absorption ability, mechanical and shape recovery behaviors) of the sponge were characterized. The active coagulation activity was evaluated by conducting RBC/platelet adhesion assays and the whole blood clotting time test. Whether the sponge can effectively manage uncontrolled coagulopathic hemorrhage from superficial and perforating wounds was explored *in vivo* by using heparinized rat tail amputation, liver superficial injury, and liver perforating wound models (Fig. 1D). Furthermore, the biodegradability of the sponge was assessed using a lysozyme degradation assay *in vitro*, and the biocompatibility was evaluated using cell counting kit-8 (CCK-8), live/dead staining,

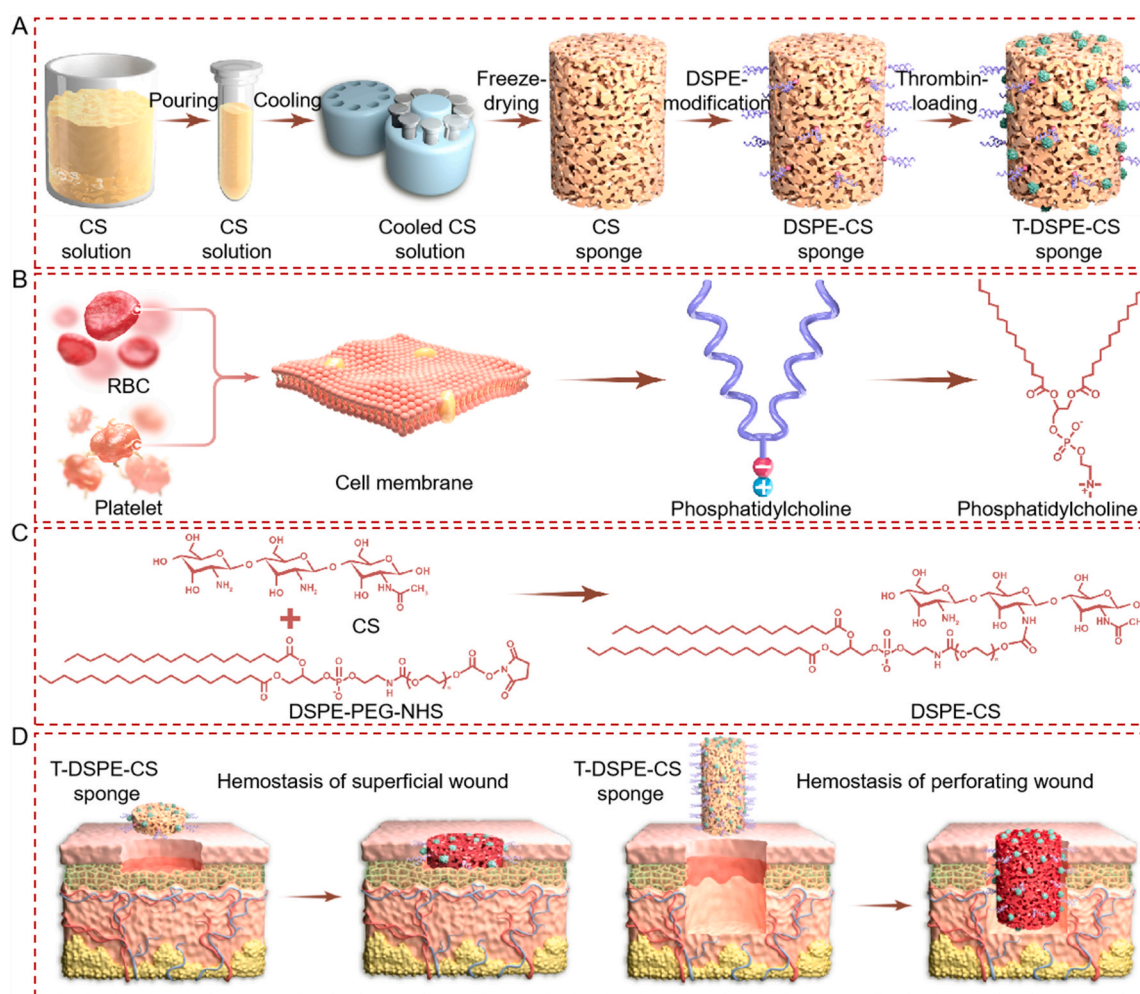


**Fig. 1.** Preparation and hemostatic applications of the thrombin-loaded DSPE-CS (T-DSPE-CS) sponge. (A) The preparation process of the T-DSPE-CS sponge. (B) The concept and (C) mechanism of DSPE-modification. (D) The hemostatic application of the T-DSPE-CS sponge in managing uncontrolled coagulopathic hemorrhage from superficial and perforating wounds.

hemolysis, and rat subcutaneous implantation tests.

## 2. Materials and methods

### 2.1. Materials

CS (molecular weight: 100 kDa, deacetylation degree: 85%) was provided by Jinan Haidebei Biotechnology Co., Ltd., China. CCK-8, live/dead staining kit, lactic dehydrogenase kit, hematoxylin-eosin (H&E) staining kit, and other chemical reagents (e.g., N,N-dimethylformamide, triethylamine, ethanol, acetic acid, glutaraldehyde) were obtained from Beijing Solarbio Science & Technology Co., Ltd., China. 1,2-Distearoyl-sn-glycero-3-phosphoethanolamine-N-[methoxy(polyethyleneglycol)] (DSPE-PEG-NHS) was purchased from Guangzhou Carbon Water Biotechnology Co., Ltd., China. Thrombin, heparin sodium, and lysozyme were provided by Sigma-Aldrich. Male Sprague-Dawley rats (weight: 250–300 g) were obtained from SPF (Beijing) Biotechnology Co., Ltd., China.

### 2.2. Preparation of the sponge

CS was dissolved in a 2% (v/v) acetic acid aqueous solution to attain a 4% (w/v) concentration. After the solution was centrifuged at 9000 rpm for 3 min, the resulting solution was added to a cylindrical mold and placed in a cell freezing container at a cooling rate of 1 °C/min. After the solution was cooled for 24 h at −18 °C, the frozen CS solution was freeze-dried to produce the porous CS sponge. Next, the sponge was immersed in 0.2 M NaOH solution to neutralize excess acetic acid and rinsed with water.

For chemical modification, the DSPE-PEG-NHS was dissolved in N,N-dimethylformamide to attain a 2% (w/v) concentration. The hydrated CS sponge was compressed to expel internal water and immersed in 10 mL of above solution. The reaction was performed for 24 h after triethylamine was added. Thereafter, the chemically modified CS (DSPE-CS) sponge was completely washed with water to remove impurities and immersed in normal saline.

For physical loading, thrombin was dissolved in normal saline to achieve a 50 UI/mL concentration. The drained DSPE-CS sponge (50 mg) was placed in a tube containing 2 mL thrombin solution. After 1 min, the thrombin-loaded DSPE-CS sponge (T-DSPE-CS) sponge was taken out and compressed to expel the internal liquid into the tube. The loading efficacy of thrombin was measured by determining the remaining thrombin in the tube using a chromogenic substrate S-2238 [5]. Considering the activity of thrombin, the T-DSPE-CS sponge did not be prepared in advance and stored. The sponge was used applying a ready-to-use principle: the DSPE-CS sponge immersed in normal saline was taken out, squeezed out water, and immersed in thrombin solution. After that, the T-DSPE-CS sponge was compressed to expel internal liquid and used immediately.

### 2.3. Chemical structure characterization

The chemical structures in both CS and DSPE-CS sponges were characterized using an X-ray photoelectron spectrometer (XPS, Thermo Scientific, ESCALAB 250Xi, USA) and Fourier transform infrared spectrometer (FTIR, Thermo Scientific, Nicolet iS20, USA).

### 2.4. Microstructure characterization

The microstructure of the sponge was observed using a scanning electron microscope (SEM, Phenom, Phenom-pro, Netherlands). The corresponding pore size was measured using Image-J software.

### 2.5. Porosity characterization

The porosity of the sponge was determined using a previous method

[27]. The weight ( $m_d$ ) and volume ( $V$ ) of the dried sponge were recorded. Then, the sponge was immersed in ethanol with a 789 kg/m<sup>3</sup> density. After the sponge was centrifuged at 9000 rpm for 10 min, the wet weight of the sponge was measured and recorded as  $m_w$ . The porosity (%) was calculated as  $(m_w - m_d) / \rho V \times 100\%$ .

### 2.6. Mechanical and injectable properties

The mechanical properties (eg., compression strength, elasticity, fatigue resistance) of the cylindrical drained sponge (11 mm in diameter, 12 mm in height) were assessed in a cyclic compression test conducted using a texture analyzer (FTC, TMS-Pro, USA). In the test, a compressive speed of 50 mm/min was applied, with compressive strains set at 30%, 50%, and 70%. The mechanical flexibility of the T-DSPE-CS sponge was evaluated in a qualitative torsion test. The injectability of the T-DSPE-CS sponge was assessed in a qualitative injection test.

### 2.7. Liquid absorption ability

The hydrated sponge was compressed to remove internal water and weighed ( $m_d$ ). The drained sponge was immersed in water or blood until an absorption equilibrium was attained, and the corresponding weight was recorded as  $m_w$ . The liquid absorption ratio (%) was calculated as  $(m_w - m_d) / m_d \times 100\%$ .

### 2.8. Shape recovery ability

The initial height of the drained sponge was measured and recorded as  $h_0$ . The sponge was subjected to longitudinal or transverse compression, and its height was noted as  $h_c$ . Following stress release, the compressed sponge returned to its original shape, and its height was recorded as  $h_r$ . The shape recovery process and time were monitored and documented. The shape compression ratio (%) was calculated as  $h_c / h_0 \times 100\%$ , and the shape recovery ratio (%) was calculated as  $h_r / h_0 \times 100\%$ .

### 2.9. The release of thrombin

The drained T-DSPE-CS sponge was immersed in 10 mL of the phosphate buffer solution (PBS, pH = 7.4) with gentle agitation at 37 °C. At predetermined time, 1 mL of the supernatant was taken out, and 1 mL of fresh PBS was added to maintain a constant volume. Then, 10 μL of the supernatant was mixed with 200 μL of reaction buffer (Tris-HCl solution with pH of 8.5 containing 20 mM of Tris and 150 mM of NaCl). After reaction for 2 min at 37 °C, 25 μL of chromogenic substrate (1 mg/mL) was added. After 6 min at 37 °C, 23.5 μL of acetic acid was added to terminate reaction. Finally, the reactant was detected by using a microplate reader at 405 nm, and pure thrombin was used as a control [5].

### 2.10. RBC adhesion assay

The whole blood was collected from rats and treated with an anti-coagulant to obtain the anticoagulated whole blood, followed by centrifuging at 3000 rpm for 15 min to obtain the packed RBC. Then, 300 μL of RBC was co-incubated with the drained sponge (or gauze and gelatin sponge serving as controls) and placed in an EP tube for 1 h at 37 °C. The sponge was fully rinsed with normal saline and transferred into 1 mL of water for 1 h. Thereafter, the absorbance ( $A_1$ ) of the supernatant at 540 nm was measured using a microplate reader. The absorbance ( $A_2$ ) of a reference solution containing packed RBC and water was also measured. The RBC adhesion ratio (%) was calculated as  $A_1 / A_2 \times 100\%$ .

The RBC adhesion was further observed through SEM. The packed RBC was co-incubated with the drained sponge for 1 h at 37 °C. The sponge was rinsed with normal saline and fixed in a 2.5% (v/v)

glutaraldehyde solution for 2 h. The fixed sponge was dehydrated in a gradient series of ethanol solutions and freeze-dried. The sponge was attached to a stage, sputter-coated with a thin layer of gold, and observed through SEM.

### 2.11. Platelet adhesion assay

The anticoagulated whole blood was centrifuged at 3000 rpm for 15 min to obtain platelet-rich plasma (PRP). First, 300  $\mu$ L of PRP was co-incubated with the drained sponge (or gauze and gelatin sponge serving as controls) and placed in an EP tube for 1 h at 37 °C. The sponge was then rinsed with normal saline and immersed into 0.1% Triton 100-X solution for 1 h. The absorbance ( $A_1$ ) of the supernatant was measured at 490 nm. The absorbance ( $A_2$ ) of a solution comprising PRP and 0.1% Triton 100-X was also measured. The platelet adhesion ratio (%) was calculated as  $A_1/A_2 \times 100\%$ .

Platelet adhesion was further observed through SEM. Then, 300  $\mu$ L of PRP was co-incubated with the drained sponge for 1 h at 37 °C. The sponge was rinsed with normal saline to remove nonadherent platelets. Next, the sponge was fixed for 2 h in a 2.5% (v/v) glutaraldehyde solution, dehydrated in a gradient series of ethanol solutions, and freeze-dried. The sponge was attached to a stage, sputter-coated with a thin layer of gold, and observed through SEM.

### 2.12. Whole blood clotting time test

The whole blood clotting time test was conducted according to a previous method [28]. First, 0.2 mL of anticoagulated whole blood from the rats was added to the drained sponge (or gauze and gelatin sponge) in a tube. Then, 0.1 mL of 0.1 M calcium chloride solution was introduced into the tube to initiate blood coagulation. Thereafter, the tube was incubated at 37 °C, and whole blood clotting was timely observed. The whole blood clotting time was determined as the time at which a uniform clot was formed in the tube.

### 2.13. In vivo hemostatic capacity

*In vivo* experiments were conducted in strict accordance with National Institutes of Health guidelines for the care and use of laboratory animals and were approved by Institutional Animal Care and Use Committee of Yi Shengyuan Gene Technology (Tianjin) Co., Ltd. (YSY-DWLL-2023221). Heparinized rat tail amputation, liver superficial injury, and liver perforating wound models were used to assess the capacity of the sponge in managing coagulatic hemorrhage from superficial and perforating wounds. Commercial gauze and gelatin sponge were used as the controls.

In the heparinized rat tail amputation experiment, the rat was restrained and anesthetized with 1.5% isoflurane. Then, the heparin sodium solution (50 UI) was administered to the rat via tail vein at a dose of 2 mL/kg. The tail was placed on the surface of a weighing filter paper ( $W_f$ ). Next, a weighing paper ( $W_w$ ) was placed beneath the filter paper to inhibit water absorption. Then, the tail was cut using a surgical instrument. Following hemorrhage, a circular drained sponge was pressed against the wound's surface. After hemostasis, the total weight of the weighing paper, filter paper, and sponge was recorded as  $W_t$ .

In the heparinized rat liver superficial injury experiment, the rat was anesthetized with 1.5% isoflurane and fixed on an operating table. Then, the heparin sodium solution (50 UI) was administered to the rat via tail vein at a dose of 2 mL/kg. The rat's abdomen was incised to expose the liver, which was then placed on the surface of a weighing paper ( $W_w$ ) and filter paper ( $W_f$ ) in turn. Thereafter, a wound (6 mm length  $\times$  5 mm deep) was made on the liver's surface. Following hemorrhage, a circular drained sponge was compressed onto the wound's surface. After hemostasis, the total weight of the weighing paper, filter paper, and sponge was recorded as  $W_t$ .

In the heparinized rat liver perforating wound experiment, the rat

was anesthetized and fixed on an operating table. Then, the heparin sodium solution (50 UI) was administered to the rat via tail vein at a dose of 2 mL/kg. Next, the rat's abdomen was incised exposing the liver, which was then placed on the surface of a weighing filter paper ( $W_f$ ). After that, a weighing paper ( $W_w$ ) was placed beneath the filter paper to avoid the penetration of body fluid. A perforating wound having an 8-mm diameter was made on the liver. Following hemorrhage, a compressed sponge was injected into the wound cavity to achieve hemostasis. The total weight of the weighing paper, filter paper, and sponge was recorded as  $W_t$ .

In *in vivo* experiments, the total blood loss (g) was calculated as ( $W_t - W_f - W_w$ ). Hemostatic time (s) was measured using a timer, and the hemostatic process was recorded using a digital camera.

### 2.14. Biodegradability evaluation

The biodegradation test of the T-DSPE-CS sponge was conducted in 10 mL of PBS containing lysozyme at concentrations of 0, 5, and 15  $\mu$ g/mL. The dried T-DSPE-CS sponge was weighted and recorded as  $m_1$ . Then, the sponge was immersed into the solutions with gentle agitation at 37 °C. The lysozyme solution was refreshed daily to ensure continuous enzyme activity. At predetermined time (0, 7, 14, and 21 days), the sponge was removed from the medium and rinsed with water, finally freeze-dried and weighed ( $m_2$ ). The relative weight (%) was calculated as  $m_2/m_1 \times 100\%$ .

### 2.15. Cytocompatibility test

The compatibility of the sponge to 3T3 fibroblast cells was evaluated through CCK-8 and live/dead staining assays, and compared with gelatin sponge. In the CCK-8 assay, a cell suspension ( $6 \times 10^4$  cells) was applied to each drained sponge surface. After incubating the sponge for 1 and 3 days at 37 °C, the CCK-8 reagent was introduced into the well and the sponge was further incubated for 2 h. The absorbance ( $A_1$ ) of the supernatant was subsequently quantified at 450 nm. The absorbance ( $A_2$ ) of the supernatant in the tissue culture plate (TCP) group was also measured as a control. The cell viability (%) was calculated as  $A_1/A_2 \times 100\%$ . In the live/dead staining assay, a cell suspension ( $6 \times 10^4$  cells) was initially added onto the surface of a round glass coverslip and incubated for overnight at 37 °C. A circular drained sponge was brought into contact with the cells. After incubating the sponge for 1 and 3 days at 37 °C, the sponge was removed. The cells were stained with the live/dead staining agent in each well for 25 min. Finally, the stained cells were observed under an inverted fluorescent microscope (ECLIPSE Ni-U, Nikon, Japan).

### 2.16. Hemolysis test

The packed RBC was diluted with PBS to obtain a 2% (v/v) RBC suspension. First, 1 mL of the RBC suspension was added to the EP tube to immerse the drained sponge. The sponge was then incubated for 1 h at 37 °C. The tube was centrifuged at 3000 rpm for 15 min to obtain the supernatant. Next, the absorbance of the supernatant was measured at 540 nm and recorded as  $A_1$ . The absorbances of water- and PBS-diluted RBC suspensions were recorded as  $A_2$  and  $A_3$ , respectively. The hemolysis ratio (%) was calculated as  $(A_1 - A_3)/(A_2 - A_3) \times 100\%$ .

### 2.17. Histocompatibility test

The histocompatibility of the sponge was determined through rat subcutaneous implantation test [20,29] and compared with that of the gelatin sponge. A rat was anesthetized with 1.5% isoflurane, and two incisions were made on both sides of its back. Two 5 mm-diameter circular drained sponges were then implanted beneath the rat's skin. After the incisions were sutured, the rat was returned to its cage and fed. After 2 weeks, the rat was anesthetized, and its blood was collected for routine

blood and serum biochemistry tests. The sponge embedded into the skin was resected, and the major organs (e.g., heart, liver, spleen, lung, and kidney) were removed for H&E staining. In addition, the weight of rat was also detected and recorded at 0, 5, 10, and 14 days.

### 2.18. Statistical analysis

All results are expressed as means  $\pm$  standard deviation. All comparisons were performed using one-way ANOVA with Tukey's multiple comparison test or unpaired *t*-test in Prism 8.0 software (GraphPad Software Inc., USA).  $P < 0.05$  was considered to indicate statistical significance. A nonsignificant difference was expressed as "ns" when  $P > 0.05$ .

## 3. Results and discussion

### 3.1. Preparation of the sponge

A self-elastic sponge that integrates active and passive hemostatic mechanisms is highly desirable for the effective management of uncontrolled coagulopathic hemorrhage. To achieve this objective, we prepared a T-DSPE-CS sponge according to the experimental procedure outlined in Fig. 1A. Initially, the 4% (w/v) CS solution was used to prepare porous CS sponge by the freeze-drying method, which was due to the superior mechanical strength, self-elasticity, and shape recovery in air of the prepared sponge (Fig. S1). Then, the alkyl chains and phosphate groups were decorated onto the CS skeleton through an amidation reaction between the amino groups of CS and the NHS groups of DSPE-PEG-NHS (Fig. 1A–C). The results of the FTIR and XPS tests confirmed the successful decoration of these groups. The absorbance peak at  $1723\text{ cm}^{-1}$ , belonging to the stretching vibration of  $-\text{CO}-\text{O}$  group of DSPE, was observed in the FTIR spectrum of the DSPE-CS sponge (Fig. 2A). The peaks, corresponding to  $\text{P}=\text{O}/\text{P}-\text{O}$  groups of DSPE, were found in the P2p spectra of the DSPE-CS sponge (Fig. 2B and C). XPS spectra of N1s showed that the substitution degree of the DSPE was about 18%, which was indicated by the decreased peak area for the  $-\text{C}-\text{NH}_2$  (Fig. 2D and E). Finally, thrombin was physically loaded into the DSPE-CS sponge through physical absorption method. The loading efficacy of thrombin in the sponge was  $0.15 \pm 0.03\text{ UI/mg}$ .

### 3.2. Microstructure, mechanical properties, liquid absorption ability, porosity, and injectability of the sponge

The porous structure of the hemostatic sponge helps in capturing blood cells, enhances blood component concentration, and optimizes coagulation factor loading [30]. The developed sponges had a porous structure (Fig. 3A), and their pore sizes were comparable, ranging from  $100 \pm 33\ \mu\text{m}$  to  $112 \pm 27\ \mu\text{m}$  (Fig. 3B). Regarding the potential issues associated with practical applications of hemostatic sponges, the mechanical properties (e.g., mechanical strength, elasticity, and fatigue resistance) of the sponge were evaluated using a cyclic compression test. The mechanical strength of the sponge improved as the compressive strain increased (Fig. 3C–E). The T-DSPE-CS sponge exhibited a mechanical strength similar to those of CS and DSPE-CS sponges, showing no significant differences (Fig. 3F–H). Moreover, the drained T-DSPE-CS sponge exhibited excellent shape recovery when exposed to 30%, 50%, and 70% strains (Fig. 3E and Supplementary Movie 1), similar to both drained CS and DSPE-CS sponges (Fig. 3C and D), indicating favorable self-elasticity. The self-elasticity primarily originated from the homogeneous elastic pore structure. Moreover, no change was observed in the maximum strength of the T-DSPE-CS sponge after two compression cycles (Fig. 3H), which indicated that no significant damage occurred to its internal porous structure and highlighted its exceptional fatigue resistance. Similar findings were observed for CS and DSPE-CS sponges (Fig. 3F and G). Additionally, the T-DSPE-CS sponge could withstand large-scale torsion, and no damage was found after releasing torsional stress (Fig. 3I and Supplementary Movie 2), revealing its superior mechanical flexibility. Similar trends in mechanical properties (e.g., mechanical strength, self-elasticity, and fatigue resistance) were found for the CS, DSPE-CS, and T-DSPE-CS sponges after absorbing water (Fig. S2). For hemostasis of deep, penetrating, and difficult-to-access wound, the hemostatic sponge must exhibit a ability to be easily delivered into the wound in a compressed state [4,7]. The large-size T-DSPE-CS sponge could be loaded into a small-size injector to achieve the overall compression of its shape (Fig. 3J and Supplementary Movie 3), attributing to its excellent mechanical flexibility. The compressed sponge could be pushed out of injector under external stress and restore its original shape in air, meaning its superior injectability. Hemostatic sponges must have a strong liquid absorption capacity to concentrate blood components and promote coagulation [31,32]. The

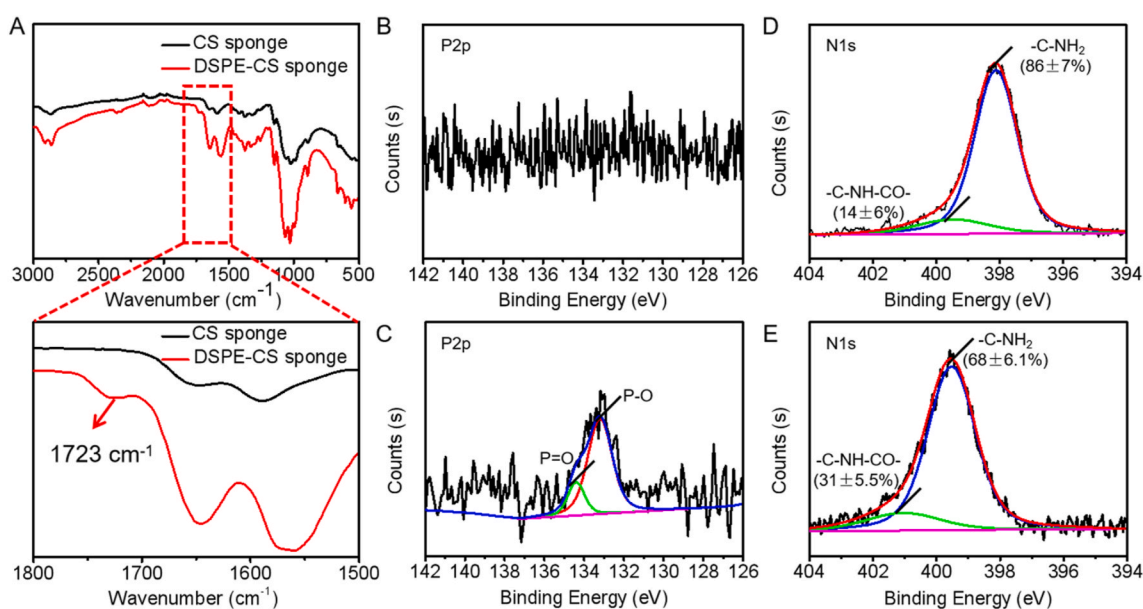


**Fig. 2.** Chemical structure characterization of the sponge. (A) FTIR spectra of the CS and DSPE-CS sponges. P2p spectra of the (B) CS sponge and (C) DSPE-CS sponge. N1s spectra of the (D) CS sponge and (E) DSPE-CS sponge.

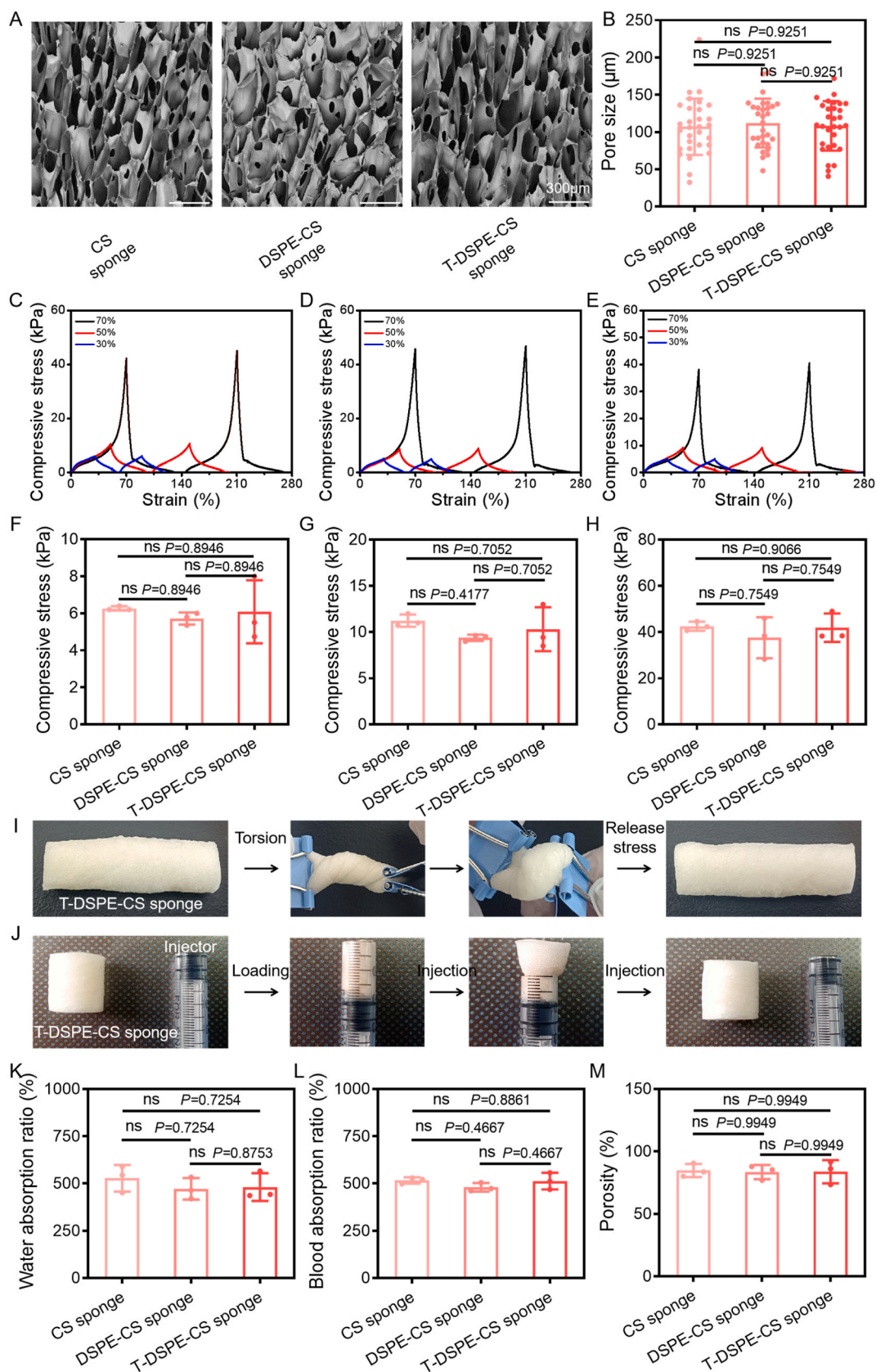


**Fig. 3.** Mechanical properties, liquid absorption ability, porosity, and injectability of the sponge. (A) SEM images and (B) corresponding pore size of the CS, DSPE-CS, and T-DSPE-CS sponges. Cyclic compressive stress-strain curves of the (C) CS, (D) DSPE-CS, and (E) T-DSPE-CS sponges at 30%, 50%, and 70% strains. Maximum compressive stresses of the CS, DSPE-CS, and T-DSPE-CS sponges at (F) 30%, (G) 50%, and (H) 70% strains. Macro photographs of the drained T-DSPE-CS sponge in the (I) torsion and (J) injection tests. (K) Water and (L) blood absorption ratios of the CS, DSPE-CS, and T-DSPE-CS sponges. (M) The porosities of the CS, DSPE-CS, and T-DSPE-CS sponges.

developed sponges could absorb liquid several times their weight (Fig. 3K and L). The water absorption ratios of the CS, DSPE-CS, and T-DSPE-CS sponges were  $528 \pm 70\%$ ,  $472 \pm 57\%$ , and  $481 \pm 73\%$ , respectively (Fig. 3K). The absorption ratios of the sponges for the blood were similar to those of the sponges for water (Fig. 3L), which indicated that their liquid absorption ability was independent on the liquid type. The T-DSPE-CS sponge exhibited an absorption ability comparable to those of CS and DSPE-CS sponges, which could be ascribed to their similar porosities (Fig. 3M). The aforementioned results demonstrate that the T-DSPE-CS sponge has favorable mechanical properties and strong liquid absorption ability, which are attributable to its self-elastic porous

structure. Moreover, the chemical modification of DSPE and physical loading of thrombin had no significant effects on the microstructure, mechanical strength, self-elasticity, and liquid absorption ability of the sponge.

### 3.3. Shape recovery ability of the sponge

The rapid shape recovery of the hemostatic sponge is positively correlated with its high hemostatic efficacy [12]. The shape recovery ability of the drained sponges was evaluated by subjecting them to longitudinal and transverse compression tests (Fig. 4). The sponges were

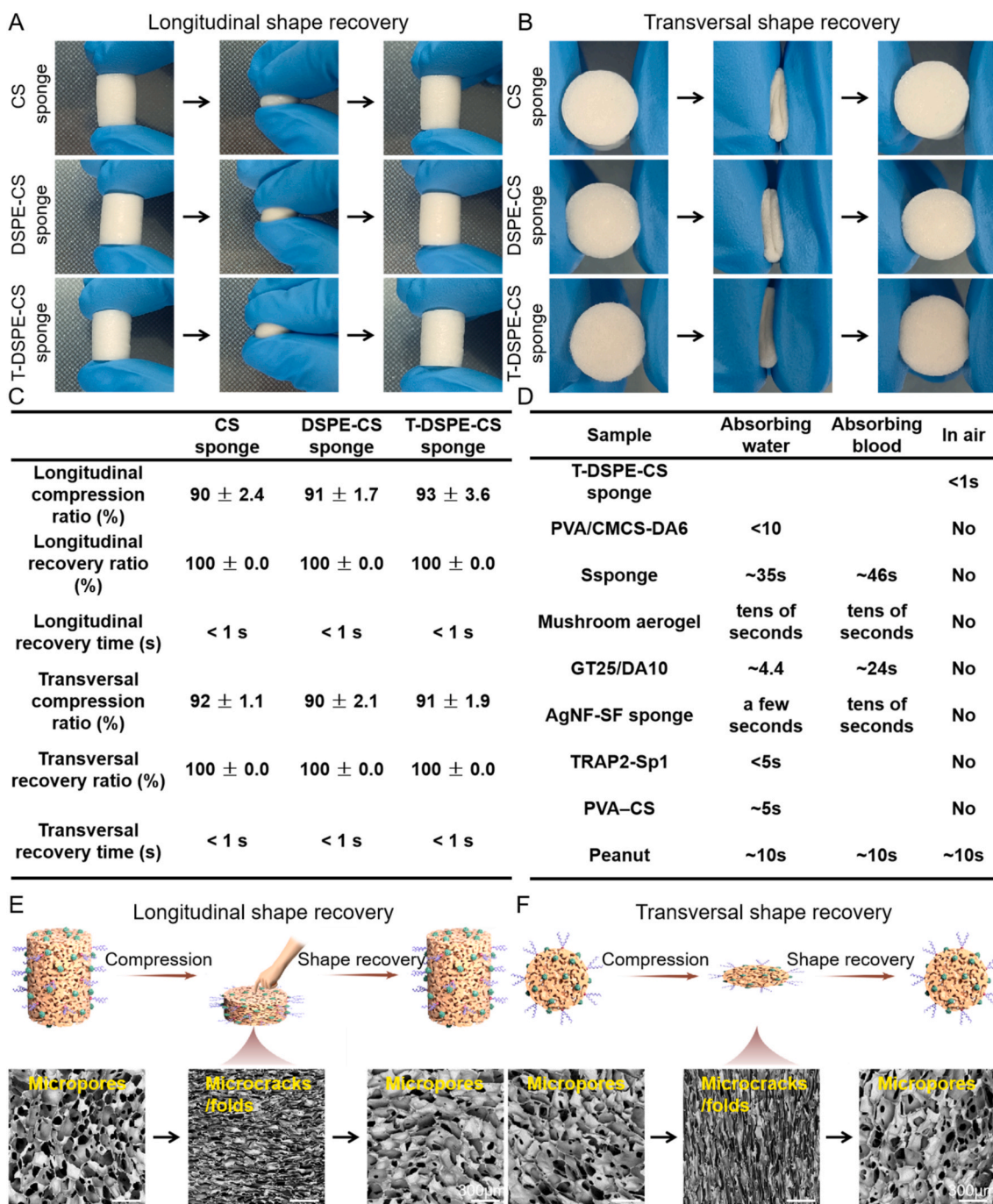


Fig. 4. Shape recovery ability of the sponge. Macro photographs of the CS, DSPE-CS, and T-DSPE-CS sponges in (A) longitudinal and (B) transversal compression tests. (C) Shape compression ratio, recovery ratio, and recovery time of the CS, DSPE-CS, and T-DSPE-CS sponges in longitudinal and transversal compression tests. (D) A comparison of shape recovery time between the T-DSPE-CS sponge and reported hemostatic sponges. Shape recovery mechanisms and SEM images of the T-DSPE-CS sponge in (E) longitudinal and (F) transversal compression tests.

compressed by  $> 90\%$ , and no significant difference was observed among the groups (Fig. 4A–C). The shape-fixed sponges immediately recovered their original shapes when the external compression stress was released (Supplementary Movies 4, 5). The sponges had a shape recovery ratio of  $100 \pm 0\%$  and a recovery time of much less than 1 s (Fig. 4C). The T-DSPE-CS sponge displayed a considerably shorter shape recovery time than the reported sponges, ranging from seconds to tens of seconds [5,6,10,19–21,32–34]. The T-DSPE-CS sponge recovered its shape because of its inherent self-elasticity, whereas the other reported sponges recovered their shape by stimulating body fluid. More importantly, the shape recovery time of the T-DSPE-CS sponge was not affected by the increased viscosity of the body fluid; however, the shape recovery of most reported sponges was significantly prolonged when they were exposed to high-viscosity body fluids (e.g., blood) (Fig. 4D). The T-DSPE-CS sponge offers greater advantages in managing uncontrolled hemorrhage, especially from perforating wounds.

Additionally, the changes in the sponge pore structure were observed through SEM (Fig. 4E and F). Before compression, the T-DSPE-CS sponge exhibited a complete microporous structure. Under longitudinal or

transverse compressive stress, the pore walls were bent, folded, and extruded against each other, thereby forming microcracks and microfolds. Once the compression stress was released, these microcracks and microfolds reverted to their original shapes, creating a microporous structure. Excellent shape recovery of the T-DSPE-CS sponge is because of the reversible change in its self-elastic porous structure under external stress.

### 3.4. The release of thrombin from the sponge

The release profile over time of thrombin from the T-DSPE-CS sponge was shown in Fig. S3. After immersion for 2 min, the release content of thrombin was  $3.3 \pm 0.6$  UI. With the increase of immersion time, thrombin could still be released continuously from the sponge. At 8 min, the release content reached  $7.0 \pm 0.3$  UI, revealing high activity of loaded thrombin. The rapid release of thrombin was related to the porous structure of the sponge and its good water solubility. Thrombin can accelerate hemostasis by promoting the conversion of soluble fibrinogen in plasma into insoluble fibrin in intrinsic coagulation

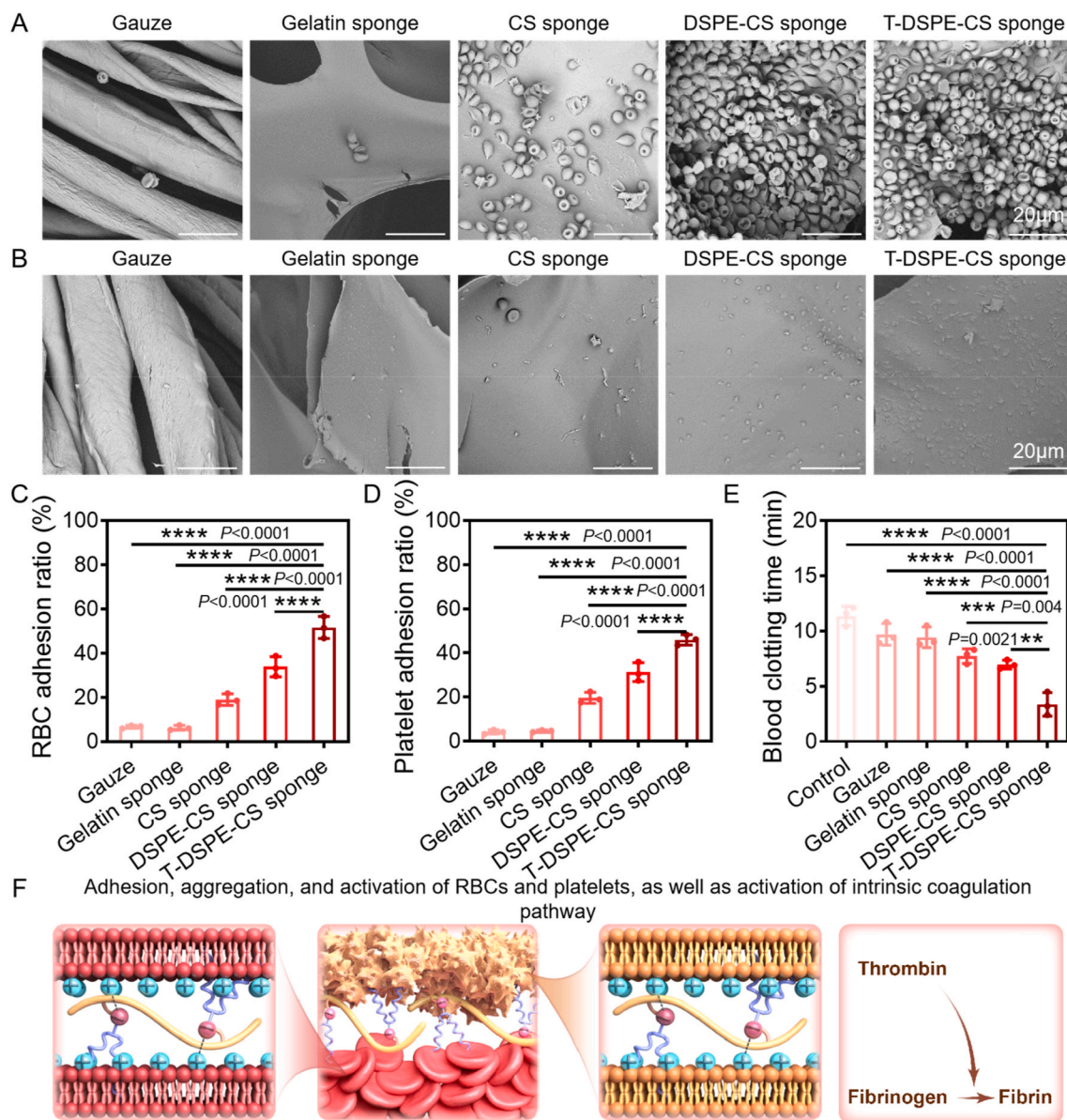


Fig. 5. *In vitro* coagulation activity of the sponge. (A, B) SEM images and (C, D) adhesion ratios of RBC and platelet on the gauze, gelatin sponge, CS sponge, DSPE-CS sponge, and T-DSPE-CS sponge, respectively. (E) Whole blood clotting time of different groups. (F) The coagulation mechanisms of the T-DSPE-CS sponge.

pathway [5]. Thus, the loading and rapid release of thrombin were conducive to increase the hemostasis efficiency of the T-DSPE-CS sponge, especially for uncontrolled coagulopathic hemorrhage.

### 3.5. In vitro coagulation activity of the sponge

RBCs and platelets are crucial players in physiological hemostasis

[24,35]. We hypothesized that the decorated alkyl chains can insert into the hydrophobic regions of cell membranes, while the decorated phosphate groups can electrostatically interact with the positive charge of their membranes. This synergistic effect promotes their adhesion, aggregation, and activation. The physical loading of thrombin accelerates blood clotting by initiating the intrinsic/exogenous coagulation cascade process (promoting the conversion of soluble fibrinogen in plasma into

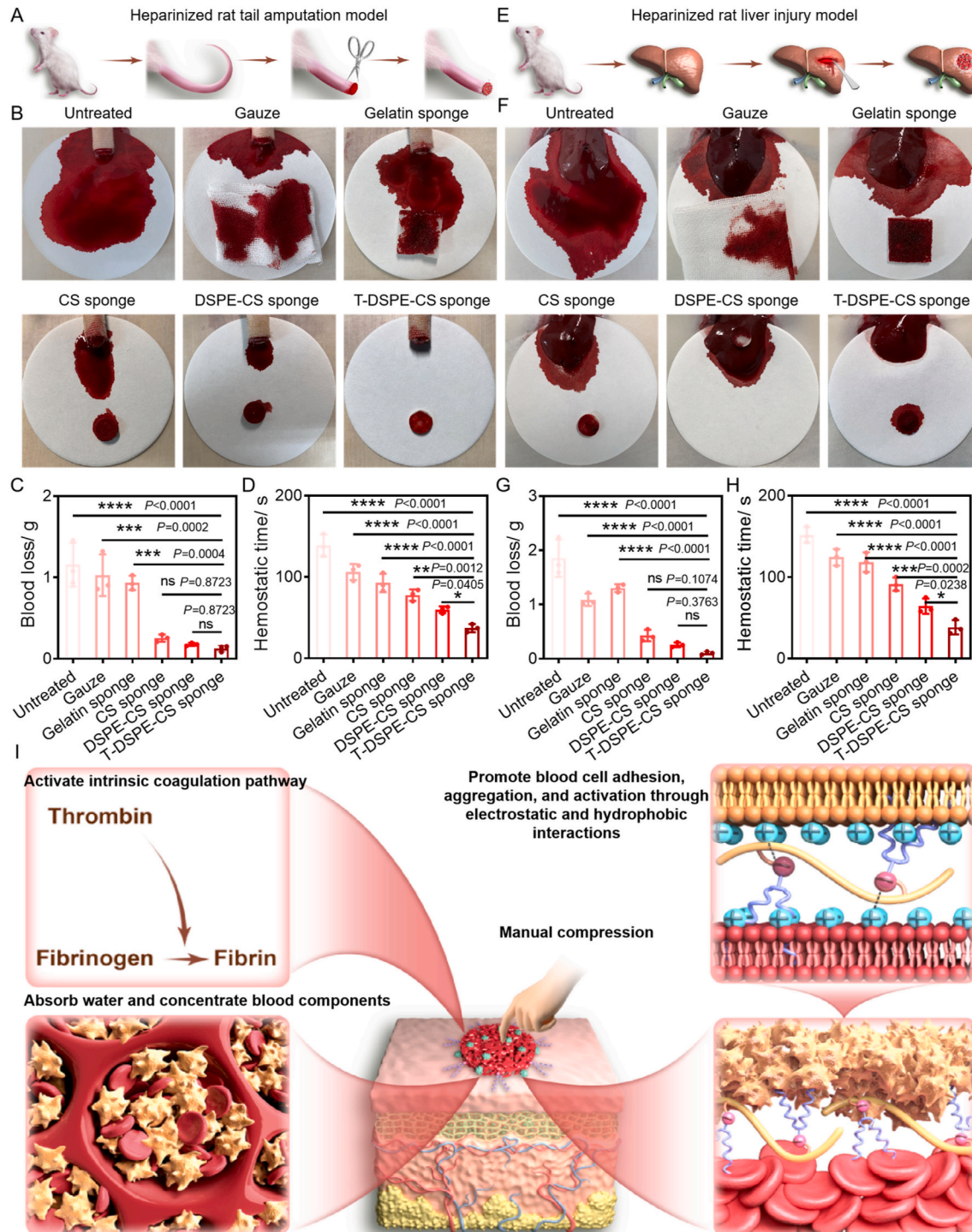


**Fig. 6.** Managing uncontrolled coagulopathic hemorrhage from superficial wounds. (A) The heparinized rat tail amputation hemostatic model. (B) Macro photographs depicting these wounds untreated and treated with hemostats. (C) Total blood loss and (D) hemostatic time of untreated and hemostats-treated groups. (E) The heparinized rat liver superficial injury hemostatic model. (F) Macro photographs of untreated and hemostats-treated wounds. (G) Total blood loss and (H) hemostatic time of untreated and hemostats-treated groups. (I) The hemostatic mechanism of the T-DSPE-CS sponge in managing uncontrolled coagulopathic hemorrhage from superficial wounds.

insoluble fibrin). This hypothesis was first verified through RBC and platelet adhesion assays. SEM images revealed that more aggregated RBCs and platelets adhered to the surface of the DSPE-CS sponge than to that of the CS sponge (Fig. 5A and B) because of the introduced alkyl chains and phosphate groups. The T-DSPE-CS sponge exhibited improved RBC and platelet adhesion and aggregation compared with the DSPE-CS sponge, contributing by the physical loading of thrombin that enabled the clotting of packed RBCs and PRP within the T-DSPE-CS sponge. Moreover, RBC and platelet adhesion and aggregation of the

T-DSPE-CS sponge were also enhanced compared with those of the commercial gauze and gelatin sponges. Additionally, the T-DSPE-CS sponge presented some polarized platelets, which indicated its ability to promote platelet activation (Fig. 5B). The quantitative results further confirmed these findings, presenting that the T-DSPE-CS sponge had a significantly higher RBC adhesion ratio of  $52 \pm 5\%$  and platelet adhesion ratio of  $46 \pm 2\%$  than the other hemostats (Fig. 5C and D). The ability of the sponges to accelerate blood clotting was assessed using a whole blood clotting time test. The T-DSPE-CS sponge had a

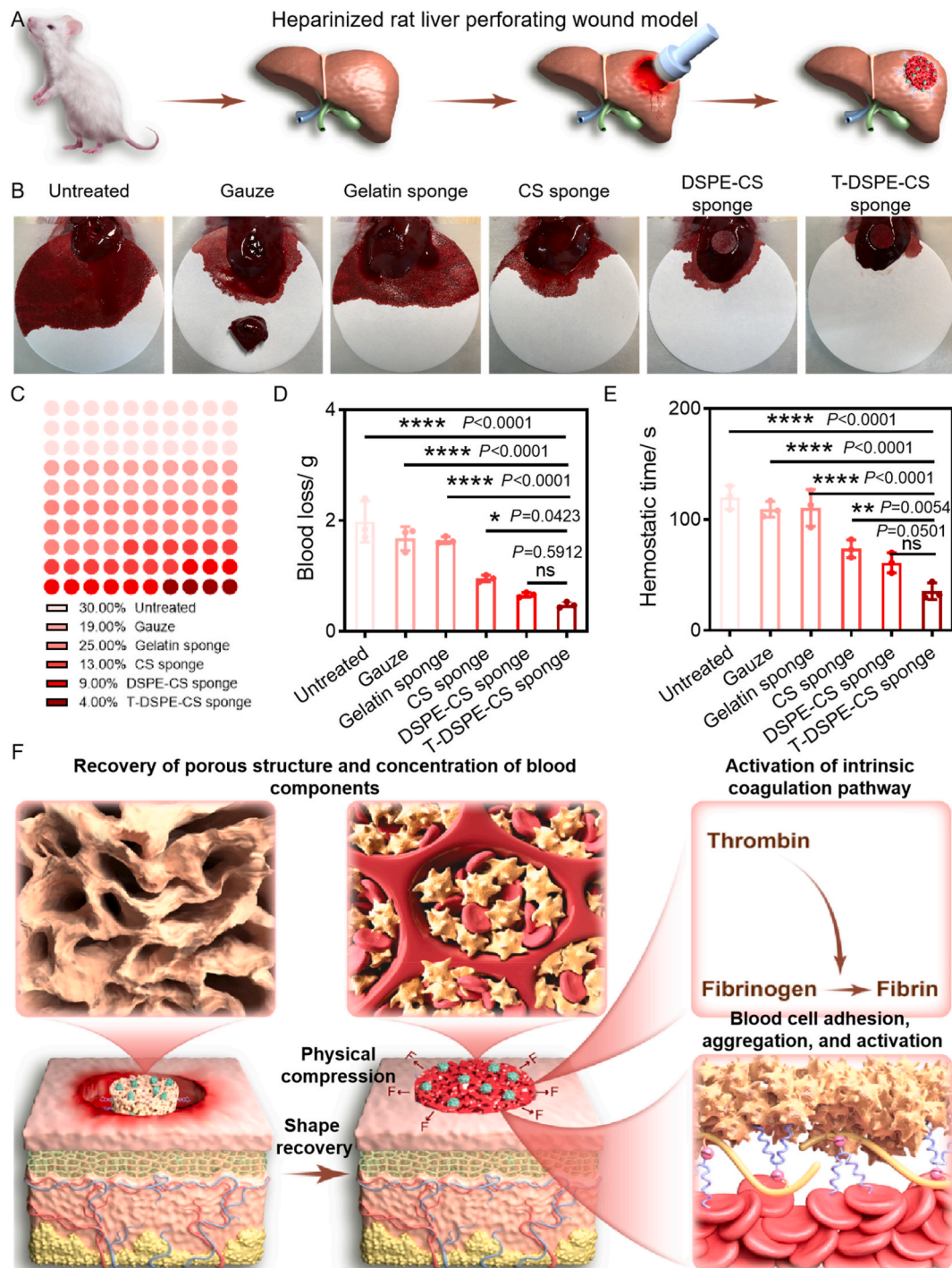


Fig. 7. Managing uncontrolled coagulopathic hemorrhage from noncompressible perforating wounds. (A) The heparinized rat liver perforating wound hemostatic model. (B) Macro photographs and (C) bloodstain area of these wounds untreated and treated with hemostats. (D) Total blood loss and (E) hemostatic time of untreated and hemostats-treated groups. (F) The hemostatic mechanism of the T-DSPE-CS sponge in managing uncontrolled coagulopathic hemorrhage from the noncompressible perforating wound.

significantly reduced whole blood clotting time of  $3.4 \pm 1.1$  min compared with the other hemostats (Fig. 5E). All the aforementioned results confirm the reasonableness and correctness of our hypothesis (Fig. 5F).

### 3.6. Managing uncontrolled coagulopathic hemorrhage from superficial wounds

To evaluate the capacity of the T-DSPE-CS sponge in managing coagulopathic uncontrolled hemorrhage from superficial wounds, a heparinized rat tail amputation model was first created and used (Fig. 6A). The T-DSPE-CS sponge-treated wound exhibited minimal blood leakage and only a small amount of blood was observed on the surface of the filter paper (Fig. 6B). By contrast, untreated wounds and those treated with the other hemostats exhibited significant blood leakage and a large amount of blood on the filter paper's surface. According to the statistical results, the T-DSPE-CS sponge group had a total blood loss of  $0.13 \pm 0.04$  g, and the untreated group, gauze, gelatin sponge, CS sponge, and DSPE-CS sponge groups had blood losses of  $1.16 \pm 0.27$  g,  $1.03 \pm 0.26$  g,  $0.93 \pm 0.09$  g,  $0.25 \pm 0.04$  g, and  $0.18 \pm 0.02$  g, respectively (Fig. 6C). Moreover, the hemostatic time of the T-DSPE-CS sponge-treated wounds was  $37 \pm 5$  s, whereas that of gauze-, gelatin sponge-, CS sponge-, and DSPE-CS sponge-treated wounds was  $106 \pm 9.8$  s,  $93 \pm 11$  s,  $78 \pm 7.1$  s, and  $60 \pm 4.2$  s, respectively (Fig. 6D).

The heparinized rat liver injury model was also established to further measure the *in vivo* hemostatic capacity of the T-DS-CS sponge (Fig. 6E). The T-DSPE-CS sponge-treated wound exhibited minimal blood leakage, with only a small amount of blood observed on the filter paper's surface (Fig. 6F). By contrast, untreated wounds and those treated with the other hemostats exhibited significant blood leakage, which led to a loss of substantial amount of blood. Consistently, significantly less total blood loss ( $0.1 \pm 0.03$  g) was noted in the T-DSPE-CS sponge group compared with the other groups, particularly the untreated, gauze, and gelatin sponge groups (Fig. 6G). Furthermore, the T-DSPE-CS sponge had a significantly reduced hemostatic time of  $38 \pm 8.7$  s compared with the other groups (Fig. 6H).

Thus, according to these results, the T-DSPE-CS sponge can effectively manage uncontrolled coagulopathic hemorrhage from superficial wounds. This is because of the synergistic effects of manual physical compression on the wound and active coagulation activity (e.g., interacting with RBCs and platelets, initiating the body's intrinsic coagulation pathway) (Fig. 6I).

### 3.7. Managing uncontrolled coagulopathic hemorrhage from noncompressible perforating wounds

The capacity of the T-DSPE-CS sponge to manage uncontrolled coagulopathic hemorrhage from perforating wound was evaluated using a heparinized rat liver perforating wound model (Fig. 7A). The T-DSPE-CS sponge-treated wound demonstrated minimal blood seepage, with only a small amount of blood observed on the filter paper's surface (Fig. 7B and C). Conversely, untreated wounds and those treated with the other hemostats exhibited severe blood leakage, leading to a loss of a considerable amount of blood. The T-DSPE-CS sponge group consistently had significantly lower levels of overall blood loss ( $0.48 \pm 0.05$  g) than the other groups (Fig. 7D). Furthermore, the T-DSPE-CS sponge had significantly reduced hemostatic time of  $35 \pm 8$  s compared with the other groups (Fig. 7E). The T-DSPE-CS sponge effectively manages uncontrolled hemorrhage from noncompressible perforating wounds because of the following factors (Fig. 7F). The compressed T-DSPE-CS sponge could return to its original shape excellently, which allowed it to serve as a physical plug that filled the wound cavity and applied mechanical pressure to control hemorrhage (Supplementary Movie 6). The T-DSPE-CS sponge could absorb water within the blood and accumulate blood components at the bleeding site, thereby promoting coagulation. The T-DSPE-CS sponge could promote the adhesion, aggregation, and

activation of RBCs and platelets through intensive hydrophobic and electrostatic interactions, facilitating blood clot formation, wound blockage, and release of coagulation factors. The release of thrombin activated the body's intrinsic coagulation cascade process, thereby enhancing hemostatic efficacy. The T-DSPE-CS sponge achieved effectively wound hemostasis through the combined action of intrinsic and exogenous or active and passive coagulation pathways.

### 3.8. Biodegradability and biocompatibility evaluation

The biodegradability of the T-DSPE-CS sponge was evaluated by a lysozyme degradation assay. As the degradation time increased, the weight of the sponge gradually decreased (Fig. 8A). The relative weight of the sponge in lysozyme groups was lower than that in PBS group, attributing to the hydrolysis effect of lysozyme to CS. Moreover, the relative weight significantly decreased with the increase of lysozyme concentration (Fig. 8A). The above results indicate that the T-DSPE-CS sponge possesses favorable biodegradability *in vitro*. It is well known that lysozyme is widely distributed in body fluids, liver, kidney, and lymphoid tissues. Therefore, we believe that the T-DSPE-CS sponge will also exhibit favorable biodegradability *in vivo*.

The hemocompatibility of the T-DSPE-CS sponge was assessed using the hemolysis test. The T-DSPE-CS sponge had a significantly lower hemolysis ratio ( $1.34 \pm 0.12\%$ ) than the water group and a ratio comparable to that of the PBS group (Fig. 8B). Furthermore, the hemolysis ratio of the T-DSPE-CS sponge was below the acceptable 5% [28], which indicates good hemocompatibility.

The cytocompatibility of the T-DSPE-CS sponge was examined in cell proliferation and live/dead staining assays. The T-DSPE-CS sponge had cell viability (>90%) comparable to that of the commercial gelatin sponge (Fig. 8C) and exhibited minimal observed dead cells after 1 and 3 days of co-culture (Fig. 8D). These results demonstrate that the T-DSPE-CS sponge had favorable cytocompatibility.

The histocompatibility of the T-DSPE-CS sponge was evaluated through the subcutaneous implantation test conducted in rats. H&E staining of the skin and other major organs (heart, liver, spleen, lung, and kidney) revealed no evident pathological differences between the T-DSPE-CS sponge and control groups (Fig. 8E). This indicated that the T-DSPE-CS sponge-induced no obverse inflammatory response. Moreover, the T-DSPE-CS sponge exhibited no significant differences in routine blood and biochemical test indices (Fig. 8F and G), as well as in rat weights (Fig. 8H) compared with the control groups. These results indicate that the T-DSPE-CS sponge has favorable *in vivo* histocompatibility.

Altogether, the findings indicate that the T-DSPE-CS sponge has favorable biodegradability *in vitro* and biocompatibility.

## 4. Conclusions

In summary, the self-elastic CS sponge integrated with active and passive hemostatic mechanisms was successfully prepared using freeze-drying, chemical modification, and physical absorption methods in combination. The sponge exhibited a microporous structure, high self-elasticity, rapid shape recovery, and good liquid absorbability. It could interact with RBCs and platelets through hydrophobic and electrostatic interactions, while also accelerating blood clotting. Moreover, the sponge exhibited favorable biodegradability *in vitro* and biocompatibility. The capability in managing uncontrolled coagulopathic hemorrhage of the sponge was demonstrated *in vivo* using heparinized rat tail amputation, liver superficial injury, and liver perforating wound models. The sponge was superior to the commercial gauze and gelatin sponge in effectively managing uncontrolled coagulopathic hemorrhage from superficial and perforation wounds.

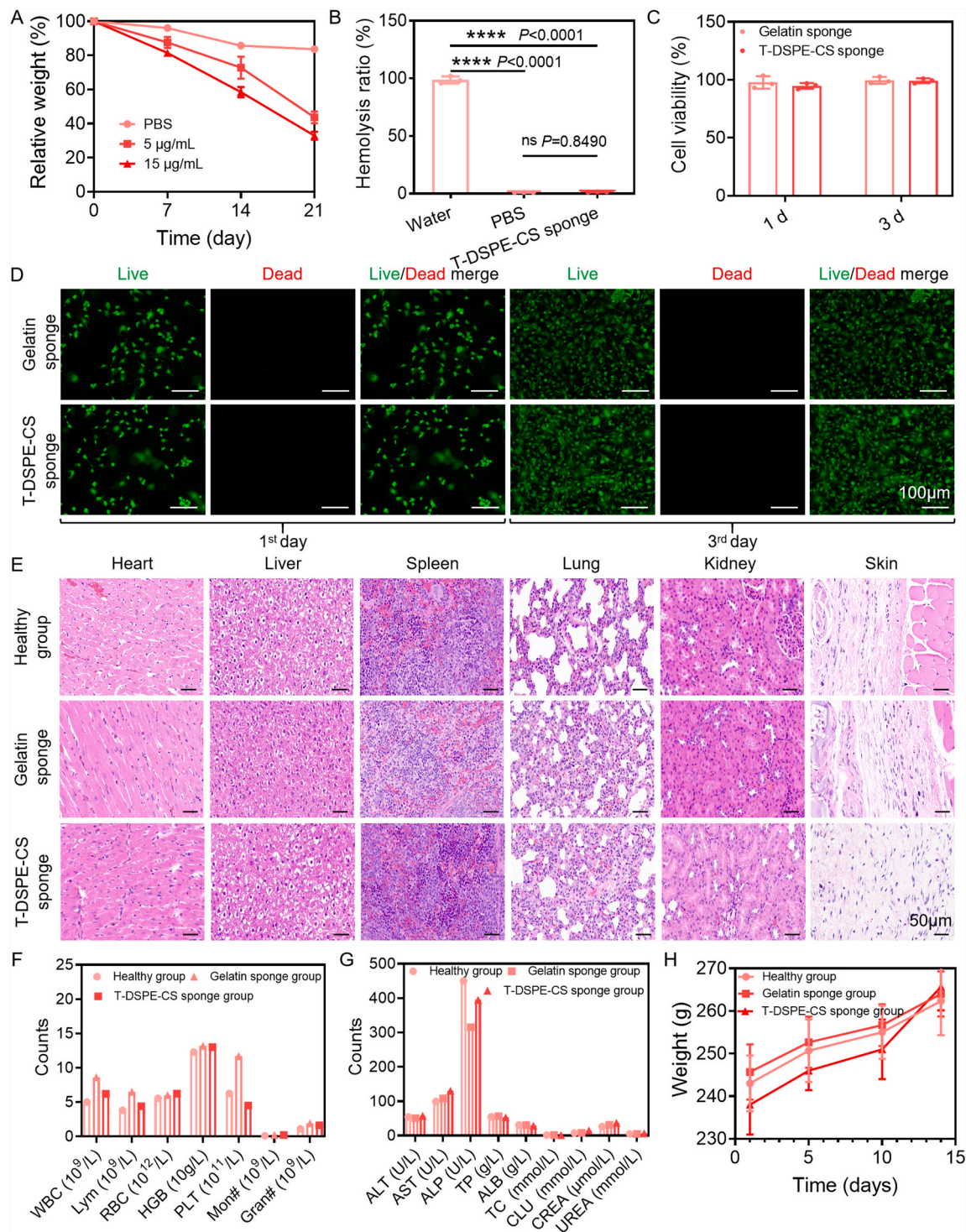


**Fig. 8.** Biodegradability and biocompatibility evaluation of the sponge. (A) The relative weight of the T-DSPE-CS sponge in PBS containing lysozyme at concentrations of 0, 5 and 15 µg/mL. (B) Hemolysis ratios of the water, PBS, and T-DSPE-CS sponge groups. (C) The cell viability and (D) Live/dead staining images in the T-DSPE-CS sponge and gelatin sponge groups after 1 and 3 days. (E) H&E staining images of the sponge embedded skin and major organs (heart, liver, spleen, lung, and kidney) in the T-DSPE-CS sponge and control groups. (F) Blood routine and (G) biochemical test indices in the T-DSPE-CS sponge and control groups. (H) The body weight variation of rats in the T-DSPE-CS sponge and control groups.

#### CRediT authorship contribution statement

**Xinchen Du:** Writing – original draft, Formal analysis, Data curation, Conceptualization. **Tongxing Zhang:** Data curation, Conceptualization. **Yadong Liu:** Data curation, Conceptualization. **Tong Li:** Data curation. **Jiuxia Yang:** Data curation. **Xueleli Li:** Writing – review & editing, Supervision, Conceptualization. **Lianyong Wang:** Writing –

review & editing, Supervision, Formal analysis.

#### Declaration of competing interest

The authors declare that they have no known competing financial interests or personal relationships that could have appeared to influence the work reported in this paper.

## Data availability

Data will be made available on request.

## Acknowledgements

This work was financially supported by the National Natural Science Foundation of China (32360233), Inner Mongolia Natural Science Foundation (2023QN03020), Hetao College High-Level Talent Introduction Project (HYRC202301, HYRC202317), and Chun Foundation of Tianjin First Central Hospital (2020CM12).

## Appendix A. Supplementary data

Supplementary data to this article can be found online at <https://doi.org/10.1016/j.mtbio.2024.101031>.

## References

- H.T. Beaman, E. Shepherd, J. Satalin, S. Blair, H. Ramcharran, S. Serinelli, L. Gitto, K.S. Dong, G. Nieman, S.G. Schauer, Hemostatic shape memory polymer foams with improved survival in a lethal traumatic hemorrhage model, *Acta Biomater.* 137 (2021) 112–123.
- K. Kim, J.H. Ryu, M.Y. Koh, S.P. Yun, S. Kim, J.P. Park, C.W. Jung, M.S. Lee, H. I. Seo, J.H. Kim, Coagulopathy-independent, bioinspired hemostatic materials: a full research story from preclinical models to a human clinical trial, *Sci. Adv.* 7 (13) (2021) eabc9992.
- Z. Zhu, K. Zhang, Y. Xian, G. He, Z. Pan, H. Wang, C. Zhang, D. Wu, A choline phosphoryl-conjugated chitosan/oxidized dextran injectable self-healing hydrogel for improved hemostatic efficacy, *Biomacromolecules* 24 (2) (2023) 690–703.
- Y. Fang, Y. Xu, Z. Wang, W. Zhou, L. Yan, X. Fan, H. Liu, 3D porous chitin sponge with high absorbency, rapid shape recovery, and excellent antibacterial activities for noncompressible wound, *Chem. Eng. J.* 388 (2020) 124169.
- X. Zhao, Y. Liang, B. Guo, Z. Yin, D. Zhu, Y. Han, Injectable dry cryogels with excellent blood-sucking expansion and blood clotting to cease hemorrhage for lethal deep-wounds, coagulopathy and tissue regeneration, *Chem. Eng. J.* 403 (1) (2021) 126329.
- X. Yang, W. Liu, Y. Shi, G. Xi, M. Wang, B. Liang, Y. Feng, X. Ren, C. Shi, Peptide-immobilized starch/PEG sponge with rapid shape recovery and dual-function for both uncontrolled and noncompressible hemorrhage, *Acta Biomater.* 99 (2019) 220–235.
- L. Yao, H. Gao, Z. Lin, A shape memory and antibacterial cryogel with rapid hemostasis for noncompressible hemorrhage and wound healing, *Chem. Eng. J.* 428 (2022) 131005.
- S.M. Andrabi, A. Kumar, A kaolin/calcium incorporated shape memory and antimicrobial chitosan-dextran based cryogel as an efficient haemostatic dressing for uncontrolled hemorrhagic wounds, *Biomaterials Adv* 150 (2023) 213424.
- X. Du, L. Wu, H. Yan, Z. Jiang, S. Li, W. Li, Y. Bai, H. Wang, Z. Cheng, D. Kong, L. Wang, M. Zhu, Microchannelled alkylated chitosan sponge to treat noncompressible hemorrhages and facilitate wound healing, *Nat. Commun.* 12 (1) (2021) 4733.
- Y. Huang, X. Zhao, C. Wang, J. Chen, B. Guo, High-strength anti-bacterial composite cryogel for lethal noncompressible hemorrhage hemostasis: synergistic physical hemostasis and chemical hemostasis, *Chem. Eng. J.* 9 (2021) 131977.
- Z. Wu, W. Zhou, W. Deng, C. Xu, Y. Cai, X. Wang, Antibacterial and hemostatic thiol-modified chitosan-immobilized AgNPs composite sponges, *ACS Appl. Mater. Inter.* 12 (18) (2020) 20307–20320.
- Z. Ren, M. Li, F. Wang, J. Qiao, M. Kaya, K. Tang, Antibacterial chitosan-based composite sponge with synergistic hemostatic effect for massive haemorrhage, *Int. J. Biol. Macromol.* 252 (2023) 126344.
- S. Li, M. Jiang, Y. Zhang, X. Xie, W. Li, P. Ming, X. Jiang, B. Yang, Y. He, J. Chen, Multi-functional carboxymethyl chitosan/sericin protein/halloysite composite sponge with efficient antibacterial and hemostatic properties for accelerating wound healing, *Int. J. Biol. Macromol.* 234 (2023) 123357.
- P. Li, L. Cao, F. Sang, B. Zhang, Z. Meng, L. Pan, J. Hao, X. Yang, Z. Ma, C. Shi, Polyvinyl alcohol/sodium alginate composite sponge with 3D ordered/disordered porous structure for rapidly controlling noncompressible hemorrhage, *Biomaterials Adv* 134 (2022) 112698.
- F. Sang, X. Yang, J. Hao, Y. Wang, X. Si, X. Li, L. Pan, Z. Ma, C. Shi, Wool keratin/zeolitic imidazolate framework-8 composite shape memory sponge with synergistic hemostatic performance for rapid hemorrhage control, *J. Mater. Chem. B* 11 (2023) 10234–10251.
- X. Wang, Q. Dang, C. Liu, G. Chang, H. Song, Q. Xu, Y. Ma, B. Li, B. Zhang, D. Cha, Antibacterial porous sponge fabricated with capric acid-grafted chitosan and oxidized dextran as a novel hemostatic dressing, *Carbohydr. Polym.* 277 (2022) 118782.
- G. Mueller, T. Pineda, H. Xie, J. Teach, A. Barofsky, J. Schmid, K. Gregory, A novel sponge-based wound stasis dressing to treat lethal noncompressible hemorrhage, *J. Trauma Acute Care* 73 (2012) S134–S139.
- S. Cao, Z. Bi, Q. Li, S. Zhang, M. Singh, J. Chen, Shape memory and antibacterial chitosan-based cryogel with hemostasis and skin wound repair, *Carbohydr. Polym.* 305 (2023) 120545.
- Y. Huang, X. Zhao, Z. Zhang, Y. Liang, Z. Yin, B. Chen, L. Bai, Y. Han, B. Guo, Degradable gelatin-based IPN cryogel hemostat for rapidly stopping deep noncompressible hemorrhage and simultaneously improving wound healing, *Chem. Mater.* 15 (2020) 6595–6610.
- Y. Zhu, L. Zhang, W. Duan, S. Martin-Saldaña, C. Li, H. Yu, L. Feng, X. Zhang, B. Du, G. Li, X. Zheng, Y. Bu, Succinic ester-based shape memory gelatin sponge for noncompressible hemorrhage without hindering tissue regeneration, *Adv. Healthc. Mater.* 12 (5) (2023) e2202122.
- G. Yang, Z. Huang, A. McCarthy, Y. Huang, J. Pan, S. Chen, W. Wan, Super-elastic carbonized mushroom aerogel for management of uncontrolled hemorrhage, *Adv. Sci.* 10 (2023) e2207347.
- X. Chen, G. Yan, M. Chen, P. Yang, B. Xu, Alkylated chitosan-attapulgite composite sponge for rapid hemostasis, *Biomaterials Adv* 153 (2023) 213569.
- B. Guo, R. Dong, Y. Liang, M. Li, Haemostatic materials for wound healing applications, *Nat. Rev. Chem* 5 (2021) 773–791.
- M. Li, Q. Dai, S. Zhu, Q. Feng, Z. Qin, H. Gao, X. Cao, An ultrafast water absorption composite cryogel containing Iron-doped bioactive glass with rapid hemostatic ability for non-compressible and coagulopathic bleeding, *Chem. Eng. J.* 469 (2023) 143758.
- J. Liu, X. Zhou, Y. Zhang, W. Zhu, A. Wang, M. Xu, S. Zhuang, Rapid hemostasis and excellent antibacterial cerium-containing mesoporous bioactive glass/chitosan composite sponge for hemostatic material, *Mater. Today Chem.* 23 (2022) 100735.
- X. Yu, Z. Liu, J. Janzen, I. Chafeeva, S. Horte, W. Chen, R.K. Kainthan, J. N. Kizhakkedathu, D.E. Brooks, Polyvalent choline phosphate as a universal biomembrane adhesive, *Nat. Mater.* (11) (2012) 468–476.
- L. Wang, Y. Zhong, C. Qian, D. Yang, G. Ma, A natural polymer-based porous sponge with capillary-mimicking microchannels for rapid hemostasis, *Acta Biomater.* 114 (2020) 193–205.
- S. Lv, M. Cai, F. Leng, X. Jiang, Biodegradable carboxymethyl chitin-based hemostatic sponges with high strength and shape memory for non-compressible hemorrhage, *Carbohydr. Polym.* 288 (2022) 119369.
- E. Yang, W. Hou, K. Liu, H. Yang, W. Wei, H. Kang, H. Dai, Multifunctional carboxymethyl chitosan/oxidized dextran/sodium alginate hydrogels as dressing for hemostasis and closure of infected wounds, *Int. J. Biol. Macromol.* 219 (2022) 1337–1350.
- Y. Liu, H. Niu, C. Wang, X. Yang, W. Li, Y. Zhang, X. Ma, Y. Xu, P. Zheng, J. Wang, K. Dai, Bio-inspired, bio-degradable adenosine 5-diphosphate-modified hyaluronic acid coordinated hydrophobic undecanate-modified chitosan for hemostasis and wound healing, *Bioact. Mater.* 17 (2023) 162–177.
- Q. Ouyang, T. Hou, C. Li, Z. Hu, L. Liang, S. Li, Q. Zhong, P. Li, Construction of a composite sponge containing tilapia peptides and chitosan with improved hemostatic performance, *Int. J. Biol. Macromol.* 139 (2019) 719–729.
- R. Haghniaz, A. Gangrade, H. Montazerian, F. Zarei, M. Ermiş, Z. Li, Y. Du, S. Khosravi, K. Mandal, A. Rashad, F. Zehtabi, J. Li, M. Dokmeci, H. Kim, A. Khademhosseini, Y. Zhu, An all-in-one transient theranostic platform for intelligent management of hemorrhage, *Adv. Sci.* 10 (24) (2023) e2301406.
- X. Yang, M. Chen, P. Li, Z. Ji, M. Wang, Y. Feng, C. Shi, Fabricating poly(vinyl alcohol)/gelatin composite sponges with high absorbency and water-triggered expansion for noncompressible hemorrhage and wound healing, *J. Mater. Chem. B* 9 (2021) 1568–1582.
- S. Chen, M. Carlson, Y. Zhang, Y. Hu, J. Xie, Fabrication of injectable and superelastic nanofiber rectangle matrices ("peanuts") and their potential applications in hemostasis, *Biomaterials* 179 (2018) 46–59.
- Mi Cai, L. Huang, S. Lv, X. Jiang, Synthesis and characterization of thermosensitive 2-hydroxypropyl-trimethylammonium chitin and its antibacterial sponge for noncompressible hemostasis and tissue regeneration, *Carbohydr. Polym.* 331 (2024) 121879.